

This is the accepted manuscript made available via CHORUS. The article has been published as:

## Electronic Stopping of Slow Protons in Oxides: Scaling Properties

D. Roth, B. Bruckner, G. Undeutsch, V. Paneta, A. I. Mardare, C. L. McGahan, M. Dosmailov, J. I. Juaristi, M. Alducin, J. D. Pedarnig, R. F. Haglund, Jr., D. Primetzhofer, and P. Bauer

Phys. Rev. Lett. **119**, 163401 — Published 20 October 2017

DOI: [10.1103/PhysRevLett.119.163401](https://doi.org/10.1103/PhysRevLett.119.163401)

# Electronic stopping of slow protons in oxides: scaling properties

D. Roth<sup>1</sup>, B. Bruckner<sup>1</sup>, G. Undeutsch<sup>1</sup>, V. Paneta<sup>2</sup>, A.I. Mardare<sup>3</sup>, C.L. McGahan<sup>4</sup>, M. Dosmailov<sup>5</sup>, J.I. Juaristi<sup>6,7,8</sup>, M. Alducin<sup>6,7</sup>, J.D. Pedarnig<sup>5</sup>, R.F. Haglund, Jr.<sup>4</sup>, D. Primetzhofer<sup>2</sup>, and P. Bauer<sup>1,6</sup>

<sup>1</sup>Johannes-Kepler Universität Linz, IEP-AOP, Altenbergerstraße 69, A-4040 Linz, Austria

<sup>2</sup>Institutionen för Fysik och Astronomi, Uppsala Universitet, Box 516, S-751 20 Uppsala, Sweden

<sup>3</sup>Institut für Chemische Technologie Anorganischer Stoffe, Johannes-Kepler Universität Linz, Altenbergerstraße 69, A-4040 Linz, Austria

<sup>4</sup>Department of Physics and Astronomy, Vanderbilt University, Nashville, Tennessee 37235, USA

<sup>5</sup>Institut für Angewandte Physik, Johannes-Kepler Universität Linz, Altenbergerstraße 69, A-4040 Linz, Austria

<sup>6</sup>Donostia International Physics Center DIPC, P. Manuel de Lardizabal 4, 20018 Donostia-San Sebastián, Spain

<sup>7</sup>Centro de Física de Materiales CFM/MPC (CSIC-UPV/EHU), P. Manuel de Lardizabal 5, 20018 Donostia-San Sebastián, Spain

<sup>8</sup>Departamento de Física de Materiales, Facultad de Químicas, Universidad del País Vasco (UPV/EHU), Apartado 1072, 20018 Donostia-San Sebastián, Spain

## Abstract

Electronic stopping of slow protons in ZnO, VO<sub>2</sub> (metal and semiconductor phases), HfO<sub>2</sub> and Ta<sub>2</sub>O<sub>5</sub> was investigated experimentally. As a comparison of the resulting stopping cross sections (SCS) to data for Al<sub>2</sub>O<sub>3</sub> and SiO<sub>2</sub> reveals, electronic stopping of slow protons does not correlate with electronic properties of the specific material such as band gap energies. Instead, the oxygen 2*p* states are decisive, as corroborated by DFT calculations of the electronic densities of states. Hence, at low ion velocities the SCS of an oxide primarily scales with its oxygen density.

- 1    **PACS Numbers:** 34.50.-s, 34.50.Bw, 61.85.+p, 77.84.Bw
- 2    **Keywords:** LEIS, electronic stopping, protons, metal oxides, vanadium dioxide, zinc oxide,
- 3    tantalum pentoxide, hafnium dioxide, aluminium oxide, silicon dioxide
- 4

1 Ions are slowed down in matter due to interaction with atomic nuclei and electrons; usually  
 2 one differentiates between nuclear and electronic stopping. For many decades, fundamental  
 3 research has been dedicated to accurate description of the relevant energy loss processes. The  
 4 understanding gained is indispensable for wide-ranging applications – space research,  
 5 material science, nuclear fusion and fission or radiation therapy [1]. In this context, a key  
 6 quantity is the mean energy loss per path length, i.e., the stopping power  $S = dE/dx$ , with  
 7 contributions due to electronic excitations,  $S_e$ , and nuclear collisions,  $S_n$ . To investigate the  
 8 interaction of ions with compound materials, the stopping cross section per atom (SCS)  
 9  $\varepsilon = S/n$  is a convenient measure, where  $n$  denotes the atomic density of the target material.

10 At high ion velocities  $v \gg v_F$  ( $v_F$  denotes the Fermi velocity of the target electrons),  $S_e$  is the  
 11 main channel for energy loss of light ions in solids and accurate theoretical models are  
 12 available [2, 3, 4]. At low ion velocities,  $v \leq v_F$ ,  $S_e$  is dominated by excitation of valence  
 13 electrons, and also  $S_n$  may contribute considerably to the overall energy dissipation rate.  
 14 When the target electrons are described as a free electron gas (FEG) of effective density  $n_e$ , as  
 15 characterized by the Wigner-Seitz radius  $r_s = (3/4\pi n_e)^{1/3}$ , electronic stopping due to electron-  
 16 hole pair excitation by the screened ion charge is velocity-proportional,  $S_e = Q(Z_1, r_s) \cdot v$  [5].  
 17 The friction coefficient  $Q$  depends on  $r_s$  and on the atomic number of the ion,  $Z_1$ . The  
 18 nonlinear calculation of  $Q$  [6] has been found to describe experimental proton stopping data  
 19 quantitatively for metals and semiconductors for low velocities, up to  $v \approx v_F$ , using effective  
 20 FEG electron densities  $r_{s,\text{eff}}$ , as derived from measured plasmon energies [7].

21 For very slow protons with  $v \ll v_F$ , deviations from velocity-proportionality of  $S_e$  were  
 22 reported for target materials featuring excitation thresholds in their electronic band structures;  
 23 in noble metals, the  $d$ -bands exhibit an excitation threshold  $E_d$  of several eV with respect to  
 24 the Fermi energy  $E_F$ , so that at energies above  $\sim 1$  keV, excitation of the  $d$ -bands becomes  
 25 more and more effective and the stopping cross section rises with steeper slope [8, 9, 10, 11,  
 26 12]. Time-dependent density-functional theory (TD-DFT) calculations of  $S_e$  of protons in Au  
 27 confirmed this interpretation [13]. For large band gap insulators, electronic stopping was  
 28 found to vanish below a threshold velocity  $v_{\text{th}}$  – e.g., for LiF (band gap  $E_{g,\text{LiF}} \approx 13.6$  eV) at  
 29 velocities lower than  $v_{\text{th}} \approx 0.1$  a.u. [14, 15]. Note that  $v_{\text{th}}$  for LiF is considerably lower than the  
 30 kink velocity for Au ( $v_k \approx 0.2$  a.u.), even though  $E_{g,\text{LiF}} \gg E_d \approx 2$  eV. For LiF, TD-DFT  
 31 calculations yielded considerably lower  $S_e$  and a threshold velocity higher than the  
 32 experimental value by a factor of  $\sim 2$  [16]. Those calculations did, however, not allow for

1 charge-exchange processes or defect production, which at grazing surface collisions had been  
2 identified as main channels of electronic losses [17, 18]. At smaller impact parameters,  
3 electron promotion in atomic collisions was suggested to be responsible for the efficient  
4 electronic stopping of protons in ionic insulators [19]. Nevertheless, a conclusive description  
5 is still missing.

6 The interplay between band gaps and electronic stopping of slow ions is complex, since  $E_g$   
7 will be modified by the electric field of the ion [20, 21]. Recently, the importance of static  
8 crystal effects (momentum transfer from the crystal) [22] and dynamic defect states (“electron  
9 elevator”) [23] has been revealed. In the band gap of Si dynamic defect states induced by a  
10 *moving* Si ion lead to a very efficient transfer of electrons from the valence band to the  
11 conduction band. This mechanism is expected to be relevant also for stopping of slow protons  
12 [23].

13 Metal oxides exist in building blocks of different sizes with widely differing numbers of  
14 valence electrons per building block,  $N_{\text{val}}$ , and exhibit more covalent bonds with smaller band  
15 gaps as compared to alkali halides [24]. In this study, we investigate systematically how in  
16 oxides proton stopping is influenced by electronic features, such as  $E_g$  or the valence electron  
17 density. To this aim, we studied electronic stopping of protons in ZnO, VO<sub>2</sub>, HfO<sub>2</sub> and Ta<sub>2</sub>O<sub>5</sub>  
18 in the range  $0.15 \text{ a.u.} \leq v \leq 0.64 \text{ a.u.}$  (500 eV – 10 keV protons) and relate these results to  
19 those obtained for SiO<sub>2</sub> [14] and Al<sub>2</sub>O<sub>3</sub> [21]. In this context, VO<sub>2</sub> is a key material to  
20 investigate the influence of  $E_g$  on  $S_e$ , due to the insulator-to-metal transition at  $\sim 67^\circ \text{C}$  [25,  
21 26]. The selection of oxides was made to cover wide ranges of band gaps,  $0 \text{ eV} \leq E_g \leq 9 \text{ eV}$ ,  
22 and one to five oxygen atoms per building block, corresponding to  $6 \leq N_{\text{val}} \leq 30$ , equivalent to  
23 valence electron densities corresponding to  $1.57 \leq r_s \leq 1.86$  (see Tab. 1).

24 The experiments were performed at the IEP in Linz employing the UHV time-of-flight low  
25 energy ion scattering (TOF-LEIS) setup ACOLISSA [27]. All samples were prepared *ex-situ*;  
26 HfO<sub>2</sub> thin films were deposited on SiO<sub>2</sub>/Si by atomic layer deposition [28]; VO<sub>2</sub> thin films  
27 were sputter deposited on Si and subsequently thermally oxidized [29]. The annealed VO<sub>2</sub>  
28 films were checked for the first-order phase transition by optical transmission (near infrared)  
29 while cycling forward and backward through the critical temperature at  $\sim 68^\circ \text{C}$ . Ta<sub>2</sub>O<sub>5</sub>  
30 samples were produced by anodization of a Ta sheet [30, 31], and ZnO samples were prepared  
31 in three different ways: thermal oxidation in air of a high purity Zn sheet, pulsed laser  
32 deposition on PET [32], and sputter deposition on glass. Time-of-flight elastic recoil detection  
33 (TOF-ERD) measurements at Uppsala University yielded the expected stoichiometry and

1 impurity concentrations below  $\sim 2\%$ . Time-of-flight medium energy ion scattering (TOF-  
2 MEIS) [33] was employed to check the homogeneity of thin film samples. TOF-LEIS spectra  
3 were recorded using hydrogen and deuterium beams (monomers and dimers) in the range of  
4  $0.5 \text{ keV/u} - 10 \text{ keV/u}$ . The projectiles impinge at normal incidence and probe the bulk  
5 properties in a depth of at least several nanometers; at a scattering angle  $\theta = 129^\circ$ , time of  
6 flight (TOF) is measured for backscattered projectiles of any charge state. From the energy-  
7 converted spectra, the electronic SCS per atom,  $\epsilon_{\text{ox}}$ , was deduced.

8 For nanometer films, thickness was determined by Rutherford backscattering spectrometry  
9 (RBS). To evaluate  $\epsilon_{\text{ox}}$ , experimental spectrum widths were compared to corresponding  
10 Monte Carlo simulations (TRBS, [34]), in order to disentangle electronic and nuclear  
11 stopping. In the simulations, a screened Coulomb potential (ZBL, [35]) was used to handle  
12 scattering in close and distant collisions;  $\epsilon_{\text{ox}}$  was optimized to reproduce the width of the  
13 experimental spectrum ([11]).

14 For ZnO, Ta<sub>2</sub>O<sub>5</sub>, and at very low ion velocities  $\epsilon_{\text{ox}}$  was deduced from the height ratio of  
15 energy spectra,  $H_{\text{ox}}/H_{\text{ref}}$ , recorded for the oxide and a reference sample (of known SCS  $\epsilon_{\text{ref}}$ )  
16 for the same primary charge (similarly as in [36]). The reference targets (polycrystalline Cu  
17 and Au) were cleaned employing  $3 \text{ keV Ar}^+$  sputtering; surface purity was checked by Auger  
18 electron spectroscopy (AES). The experimental height ratios were compared to results from  
19 corresponding TRBS simulations;  $\epsilon_{\text{ox}}$  was evaluated close to the high energy edge of the  
20 spectrum, where the shapes of the experimental spectra are perfectly reproduced [37]. In the  
21 simulations,  $\epsilon_{\text{ox}}$  is the only parameter to be optimized. The statistical uncertainties of  $\epsilon_{\text{ox}}$  range  
22 from  $< 7\%$  (evaluation of spectrum widths) to  $10\% - 15\%$  (evaluation of spectrum heights),  
23 with highest uncertainties at lowest ion velocities. Systematic errors due to  $\epsilon_{\text{ref}}$  or thin film  
24 thickness determination, and the interaction potential in the simulations are  $< 10\%$ .

25 In Fig. 1,  $\epsilon_{\text{ox}}$  is shown for metallic and semiconducting VO<sub>2</sub> for H ions (protons and  
26 deuterons), measured at 300 K and 373 K, respectively, with identical  $\epsilon_{\text{ox}}$ -values for both  
27 phases. Thus, in VO<sub>2</sub> proton stopping [38] is independent of the existence of a band gap,  $E_g$ .  
28 This finding is corroborated when comparing the results for VO<sub>2</sub>, HfO<sub>2</sub> ( $E_g \approx 5.5 \text{ eV}$ ) and  
29 SiO<sub>2</sub> ( $E_g \approx 9 \text{ eV}$ ), since all  $\epsilon_{\text{ox}}$  data coincide within experimental uncertainty (see Fig. 2a).  
30 Apparently, for the investigated binary oxides, band gaps are irrelevant for electronic stopping  
31 even at low ion velocities, where energy transfers in a ion-electron collisions are small.

1 For oxides, there is no simple correspondence between valence electron densities, plasmon  
 2 energies and electronic stopping: e.g., for ZnO the experimental plasmon energy [39] is  
 3 consistent with the valence electron density, while for protons  $\varepsilon$  is lower by a factor of  $\sim 2$   
 4 than anticipated for a FEG [6] (for  $v = 0.2$  a.u.). Moreover, the SCS data spread much more  
 5 than one would anticipate from their  $r_s$  values (see Tab. 1, [6]). Clearly, it does not make  
 6 sense to describe oxides as FEG.

7 While it is easily possible at high ion velocities to relate electronic stopping of a compound,  
 8  $\varepsilon_{A_xB_{1-x}}$ , to the SCS of the constituents,  $\varepsilon_A$  and  $\varepsilon_B$ , by applying Bragg's rule [40],  $\varepsilon_{A_xB_{1-x}} = x \cdot \varepsilon_A$   
 9  $+(1-x) \cdot \varepsilon_B$ , this is a doubtful approach at low ion velocities, where formation of a compound  
 10 changes the valence electron states considerably. The breakdown of the additivity rule can be  
 11 seen in Fig. 2a, where the low velocity SCS of selected oxides (ZnO, VO<sub>2</sub>, SiO<sub>2</sub>, HfO<sub>2</sub>, Al<sub>2</sub>O<sub>3</sub>,  
 12 Ta<sub>2</sub>O<sub>5</sub>) are presented together with Bragg's rule predictions using data from [36, 41, 42, 43]:  
 13 the additivity rule results are high by more than a factor of 2 at lowest velocities, with largest  
 14 discrepancies for ZnO and SiO<sub>2</sub>.

15 In Fig. 2b, we present our results for the oxides as SCS per oxygen atom,  $\varepsilon_O = \varepsilon_{Ox} \cdot (1-x)$ , i.e.,  
 16 we relate  $\varepsilon_{Ox}$  to the oxygen sub-lattice. In this way, all data coincide within experimental  
 17 uncertainties, except for ZnO, for which  $\varepsilon_{Ox}$  rises with steeper slope at  $v \geq 0.25$  a.u., due to the  
 18 contribution from the full  $d$ -band, as for metallic Zn [41]. In fact, in oxides  $A_xO_{1-x}$ , the SCS is  
 19 proportional to the atomic fraction of oxygen,  $1-x$ , while detailed electronic properties such as  
 20 band gap energy or valence electron density are not relevant. At higher ion velocities, such a  
 21 behavior has been observed for Al<sub>2</sub>O<sub>3</sub>, SiO<sub>2</sub> and H<sub>2</sub>O ice [44] as well as for HfO<sub>2</sub> versus SiO<sub>2</sub>  
 22 [28] and traced back to an O  $2p^6$  configuration as if in oxides the ionic character of the local  
 23 bonds would prevail. At low ion velocities, however, details of the density of states (DOS)  
 24 might be highly relevant, since even the subtle differences between specific metals have clear  
 25 impact on the observed  $S_e$ , e.g., for Au and Pt [10, 11]. In order to obtain quantitative  
 26 information on the unperturbed electronic density of states, density functional (DFT)  
 27 calculations of the DOS of all presented oxides were performed with the VASP code [45, 46].  
 28 For the metallic rutile structure of VO<sub>2</sub> the PBE exchange correlation functional was used  
 29 [47]. For the monoclinic structure of VO<sub>2</sub> we used a PBE + U approach with  $U = 3.5$  eV. For  
 30 all other oxides, the hybrid PBE0 exchange correlation functional was employed [48]. In all  
 31 calculations, the energy cutoff for the plane wave basis sets is 400 eV and projector  
 32 augmented wave (PAW) potentials were utilized [49, 50]. The Brillouin zone is sampled by a  
 33  $11 \times 11 \times 11$  Monkhorst-Pack grid of  $\mathbf{k}$ -points [51] for monoclinic VO<sub>2</sub>, a  $7 \times 7 \times 11$  grid for

1 rutile  $\text{VO}_2$ , and a  $7 \times 7 \times 7$  grid for the other oxides. In evaluating the DOS, the occupancies  
 2 of the electronic states are determined with the tetrahedron method.  
 3 The results for the oxides of interest in terms of DOS per oxygen atom, DOS/O, are shown as  
 4 function of  $E - E_{\text{VB}}$  in Fig. 3, where  $E_{\text{VB}}$  represents the highest occupied state of the valence  
 5 band. Integration of the DOS per oxygen atom from  $-10$  eV up to  $E_{\text{VB}}$  yields  $\sim 6$  electrons for  
 6 all oxides, with the exception of ZnO (see below). Integration of the unoccupied DOS per  
 7 oxygen atom in an interval of 10 eV beyond the band gap is rather independent of the  
 8 metal/semiconductor atom (4 to 6 electrons). Thus, the observed scaling properties of  $\varepsilon$  may  
 9 be interpreted in a similar way as electronic stopping of protons in metals [36]. Another  
 10 aspect of these results is that for stopping of slow protons in an oxide  $\text{A}_x\text{O}_{1-x}$ , Bragg's rule is  
 11 simplified since the contribution of the cations,  $\varepsilon_{\text{A}}$ , can be set to zero.  
 12 In contrast to metals, however, a linear fit to  $\varepsilon_0$  yields an apparent velocity threshold of  
 13  $v_{\text{th}} \approx 0.055$  a.u. (even for the metallic phase of  $\text{VO}_2$ ), independent of the (unperturbed) band  
 14 gap. It is not yet clear how the existence of an apparent threshold should be interpreted [20,  
 15 21, 22, 23]. In fact, the apparent threshold velocity of  $\sim 0.055$  a.u. is comparable to those  
 16 observed for ionic crystals such as LiF ( $v_{\text{th}} \approx 0.1$  a.u.) or KCl ( $v_{\text{th}} \approx 0.07$  a.u.) [14], and for a  
 17 covalent semiconductor like Ge ( $v_{\text{th}} \approx 0.026$  a.u.) [37, 52]. It remains unclear, whether the  
 18 lack of correlation between  $v_{\text{th}}$  and  $E_{\text{g}}$  points towards a Coulomb collision with an electron in  
 19 a strongly perturbed band, towards a different process like the “electron elevator”, or towards  
 20 electron promotion in an atomic collision. In any case, the energy loss mechanism appears to  
 21 be similar for all oxides. It may be interesting to compare the response of the electronic  
 22 system to energy deposition by a slow ion and by laser pulses: when exposed to high power  
 23 femtosecond laser pulses the band gap in  $\text{VO}_2$  collapses instantaneously [53].  
 24 To conclude, we present electronic stopping data  $\varepsilon_{\text{ox}}$  for slow protons in selected oxides with  
 25 a wide range of electronic properties, e.g., band gaps from 0 eV up to 9 eV, and 6 to 30  
 26 valence electrons per building block. Our data reveal that  $\varepsilon_{\text{ox}}$  is independent of  $E_{\text{g}}$ , but scales  
 27 with the atomic fraction of oxygen in the building block, since all oxides studied exhibit  $\sim 6$   
 28 valence electrons per O atom, as corroborated by DFT-calculations of the electronic DOS –  
 29 even if the chemical bonds are only partly ionic. The irrelevance of  $E_{\text{g}}$  may be either due to a  
 30 strong modification of the electronic band structure or to dynamic defect states induced in the  
 31 band gap by the ion – causing a locally reduced band gap (“metallization”). Nevertheless, to  
 32 describe the valence electrons in the oxides as a FEG of effective density is not an expedient  
 33 approach. In any case, the present results permit to fix the electronic stopping of any oxide of



1 interest. This is important, for instance, when estimating the electron yield emitted from the  
2 first wall of a nuclear fusion device, or to determine the mean range of slow protons in an  
3 oxide. Another observation is that our  $\varepsilon_0$  data extrapolate to an apparent velocity threshold,  
4  $v_{\text{th}} \approx 0.055$  a.u., even for the metallic phase of  $\text{VO}_2$  - it simply seems to be an oxygen  
5 property. Definite answers require theoretical models with realistic description of ion-electron  
6 interactions inside band gap materials.

7 Financial support of this work by the FWF (FWF-Project No. P22587-N20 and FWF-Project  
8 No. P25704-N20) is gratefully acknowledged. MA and JIJ acknowledge financial support by  
9 the Gobierno Vasco-UPV/EHU project IT756-13, and the Spanish Ministerio de Economía y  
10 Competitividad (Grants No. FIS2013-48286-C02-02-P and FIS2016-76471-P). Fabrication  
11 and characterization of  $\text{VO}_2$  films at Vanderbilt University (CMG and RFH) was supported  
12 by a grant from the National Science Foundation (DMR-1207507). A research infrastructure  
13 fellowship of the Swedish Foundation for Strategic Research (SSF) under Contract No.  
14 RIF14-0053 supporting accelerator operation is acknowledged. PB expresses his gratitude for  
15 the kind hospitality at the DIPC in San Sebastián. We are grateful to Len Feldman, Pedro  
16 Echenique, Andres Arnau and Peter Zeppenfeld for inspiring discussions.

17

## 1 References and remarks:

- 
- [1] A. Vantomme, Nucl. Instr. Meth. B **371**, 12-26 (2016).
- [2] C.P. Race, D.R. Mason, M.W. Finnis, W.M.C. Foulkes, A.P. Horsfield, and A.P. Sutton, Rep. Prog. Phys **73**, 116501 (2010).
- [3] P. Sigmund, Particle Penetration and Radiation Effects – General Aspects and Stopping of Swift Point Charges (Springer Verlag, Berlin-Heidelberg, 2006).
- [4] J.F. Ziegler, J. Appl. Phys. **85**, 1249 (1999).
- [5] E. Fermi and E. Teller, Phys. Rev **72**, 399-408 (1947).
- [6] P.M. Echenique, R.M. Nieminen, and R.H. Ritchie, Solid State Commun. **37** (10), 779-781 (1981).
- [7] A. Mann and W. Brandt, Phys. Rev. B **24**, 4999-5003 (1981).
- [8] Velocities and lengths are given in atomic units:  $v_0 = c/137$  ( $c$  denotes the speed of light), and the Bohr radius  $a_0 = 0.529\text{\AA}$ , respectively. For protons with a kinetic energy of 25 keV,  $v = v_0$ .
- [9] J.E. Valdes, J.C. Eckardt, G.H. Lantschner, and N.R. Arista, Phys. Rev. A **49**, 1083-1088 (1994).
- [10] S.N. Markin, D. Primetzhofer, M. Spitz, and P. Bauer, Phys. Rev. B **80**, 205105 (2009).
- [11] D. Goebel, D. Roth, and P. Bauer, Phys. Rev. A **87**, 062903 (2013).
- [12] E.D. Cantero, G.H. Lantschner, J.C. Eckardt, and N.R. Arista, Phys. Rev. A **80**, 032904 (2009).
- [13] M.A. Zeb, J. Kohanoff, D. Sánchez-Portal, A. Arnau, J.I. Juaristi, and E. Artacho, Phys. Rev. Lett. **108**, 225504 (2012).
- [14] S.N. Markin, D. Primetzhofer, and P. Bauer, Phys. Rev. Lett. **103**, 113201 (2009).
- [15] L.N. Serkovic Loli, E.A. Sánchez, O. Grizzi, and N.R. Arista, Phys. Rev. A **81**, 022902 (2010).
- [16] J.M. Pruneda, D. Sánchez-Portal, A. Arnau, J.I. Juaristi, and E. Artacho, Phys. Rev. Lett. **99**, 235501 (2007).
- [17] C. Auth, A. Mertens, H. Winter, and A. Borisov, Phys. Rev. Lett. **81**, 4831 (1998).
- [18] P. Roncin, J. Villette, J. P. Atanas, and H. Khemliche, Phys. Rev. Lett. **83**, 864 (1999).

- 
- [19] P.A. Zeijlmans van Emmichoven, A. Niehaus, P. Stracke, F. Wiegershaus, S. Krischok, V. Kempter, A. Arnau, F.J. Garcia de Abajo, and M. Penalba, Phys. Rev. B **59**, 10950 (1999).
- [20] B. Solleder, L. Wirtz, and J. Burgdörfer, Phys. Rev. B **79**, 125107 (2009).
- [21] K. Eder, D. Semrad, P. Bauer, R. Golser, P. Maier-Komor, F. Aumayr, M. Peñalba, A. Arnau, J.M. Ugalde, and P.M. Echenique, Phys. Rev. Lett. **79**, 4112 (1997).
- [22] E. Artacho, J. Phys. Condens. Matter **19**, 275211 (2007).
- [23] A. Lim, W.M.C. Foulkes, A.P. Horsfield, D.R. Mason, A. Schleife, E.W. Draeger, and A.A. Correa, Phys. Rev. Lett. **116**, 043201 (2016).
- [24] W.D. Grobman, D.E. Eastman, and M.L. Cohen, Phys. Lett. **43A**, 1, 49-50 (1973).
- [25] F.J. Morin, Phys. Rev. Lett. **3**, 34 (1959).
- [26] C. Weber, D.D. O'Regan, N.D.M. Hine, M.C. Payne, G. Kotliar, and P.B. Littlewood, Phys. Rev. Lett. **108**, 256402 (2012).
- [27] M. Draxler, S.N. Markin, S.N. Ermolov, K. Schmid, C. Hesch, R. Gruber, A. Poschacher, M. Bergsmann, and P. Bauer, Vacuum **73**, 39-45 (2004).
- [28] D. Primetzhofer, Phys. Rev. A **89**, 032711 (2014).
- [29] R.E. Marvel, R.R. Harl, V. Craciun, B.R. Rogers, and R.F. Haglund, Jr., Acta Materialia **91**, 217-226 (2015).
- [30] A.W. Hassel and D. Diesing, Thin Solid Films **414**, 296-303 (2002).
- [31] J.P. Kollender, M. Voith, S. Schneiderbauer, A.I. Mardare, and A.W. Hassel, J. Electroanal. Chem. **740**, 53-60 (2015).
- [32] M. Dosmailov, L.N. Leonat, J. Patek, D. Roth, P. Bauer, M.C. Scharber, N.S. Sariciftci, and J.D. Pedarnig, Thin Solid Films **591** (A), 97-104 (2015).
- [33] M.K. Linnarsson, A. Hallén, J. Åström, D. Primetzhofer, S. Legendre, and G. Possnert, Rev. Sci. Instr. **83**, 095107 (2012).
- [34] J.P. Biersack, E. Steinbauer, and P. Bauer, Nucl. Instr. Meth. B **61**, 77-82 (1991).
- [35] J.F. Ziegler, J.P. Biersack and U. Littmark, *The stopping and range of ions in solids*, (Pergamon Press, New York, 1985), Vol. 1.

- 
- [36] D. Roth, B. Bruckner, M.V. Moro, S. Gruber, D. Goebel, J.I. Juaristi, M. Alducin, R. Steinberger, J. Duchoslav, D. Primetzhofer, and P. Bauer, Phys. Rev. Lett. **118**, 103401 (2017).
- [37] D. Roth, D. Goebel, D. Primetzhofer, and P. Bauer, Nucl. Instr. Meth. B **317**, 61-65 (2013).
- [38] Since no isotope or vicinage effects are observed, we refer in the discussion for the projectiles as to protons.
- [39] R.L. Hengehold, R.J. Almassy, and F.L. Predrotti, Phys. Rev. B **1**, 4784-4791 (1971).
- [40] W.H. Bragg and R. Kleeman, Phil. Mag. **10**, 318 (1905).
- [41] D. Goebel, W. Roessler, D. Roth, and P. Bauer, Phys. Rev. A **90**, 042706 (2014).
- [42] D. Primetzhofer, S. Rund, D. Roth, D. Goebel, and P. Bauer, Phys. Rev. Lett. **107**, 163201 (2011).
- [43] J. F. Ziegler, J. P. Biersack, and M. D. Ziegler, *SRIM, The Stopping and Range of Ions in Matter*, (SRIM Company, Chester, 2008).
- [44] P. Bauer, R. Golser, F. Aumayr, D. Semrad, A. Arnau, E. Zarate, and R. Diez-Muiño, Nucl. Instr. Meth. B **125**, 102-105 (1997).
- [45] G. Kresse and J. Furthmüller, Comput. Mater. Sci. **6**, 15 (1996).
- [46] G. Kresse and J. Furthmüller, Phys. Rev. B. **54**, 11169 (1996).
- [47] J.P. Perdew, K. Burke, and M. Ernzerhof, Phys. Rev. Lett. **77**, 3865 (1996).
- [48] C. Adamo and V. Barone, J. Chem. Phys. **110**, 6158 (1999).
- [49] P.E. Blöchl, Phys. Rev. B **50**, 17953 (1994).
- [50] G. Kresse and D. Joubert, Phys. Rev. B **59**, 1758 (1999).
- [51] H.J. Monkhorst and J.D. Pack, Phys. Rev. B **13**, 5188 (1976).
- [52] R. Ullah, F. Corsetti, D. Sánchez-Portal, and E. Artacho, Phys. Rev. B **91**, 125203 (2015).
- [53] D. Wegkamp, M. Herzog, L. Xian, M. Gatti, P. Cudazzo, C.L. McGahan, R.E. Marvel, R.F. Haglund, Jr., A. Rubio, M. Wolf, and J. Stähler, Phys. Rev. Lett. **113**, 216401 (2014).

**List of figure and table captions:**

TAB. 1: Electronic properties of ZnO, VO<sub>2</sub>, HfO<sub>2</sub>, SiO<sub>2</sub>, Al<sub>2</sub>O<sub>3</sub> and Ta<sub>2</sub>O<sub>5</sub>:  $E_g$ ,  $N_{val}$ ,  $r_s$  derived from  $n_{val} = N_{val} \cdot n$ , and experimental values  $\epsilon_{ox,expt}$  for  $v = 0.2$  a.u. (1 keV protons).

FIG. 1:  $\epsilon_{ox}$  of VO<sub>2</sub> for H ions (protons and deuterons) in both, metallic (open symbols) and semiconducting phases (full symbols) are shown as function of the ion velocity. Evaluation of both, widths and heights of the spectra, yields concordant results (see legend). The upper labelling of the abscissa denotes the corresponding proton energy.

FIG. 2:

a) For ZnO, VO<sub>2</sub>, Ta<sub>2</sub>O<sub>5</sub>, HfO<sub>2</sub>, Al<sub>2</sub>O<sub>3</sub> [21], and SiO<sub>2</sub> [14] experimental proton stopping cross section data,  $\epsilon_{ox}$  per atom, are displayed as a function of the ion velocity (full symbols), together with Bragg's rule predictions using data from [36, **Error! Bookmark not defined.** 41, 42, 43].

b) The experimental data of Fig. 2a are shown as  $\epsilon_O$  per O atom,  $\epsilon_O = \epsilon_{ox} \cdot (1-x)$ , in a wider velocity range. For HfO<sub>2</sub>, also data from Ref. [28] are shown which exhibit excellent agreement with the present results. The upper labelling of the abscissa denotes the corresponding proton energy.

FIG. 3: Electronic densities of states (DOS) per O atom for selected oxides (for VO<sub>2</sub> both metallic rutile and semiconducting monoclinic phases) are depicted as function of  $E - E_{VB}$ . For ZnO, the high DOS below -4.8 eV has been scaled down by a factor 2.5. "Zero" unoccupied DOS at higher energies is due to a limited number of bands used in the calculations.

**Tables:**

Oxide	$E_g$ (eV)	$N_{\text{val}}$	$r_s$ (a.u.)	$\epsilon_{\text{ox,expt}}(0.2 \text{ a.u.})$ ( $10^{-15} \text{ eVcm}^2/\text{atom}$ )
VO <sub>2</sub>	0 ... 0.7	13	1.58	2.33
ZnO	3.4	6	1.86	1.60
Ta <sub>2</sub> O <sub>5</sub>	3.9	30	1.69	2.71
HfO <sub>2</sub>	5.5	12	1.69	2.62
Al <sub>2</sub> O <sub>3</sub>	8	18	1.57	2.00
SiO <sub>2</sub>	9	12	1.72	2.10

Tab. 1

**Figures:**

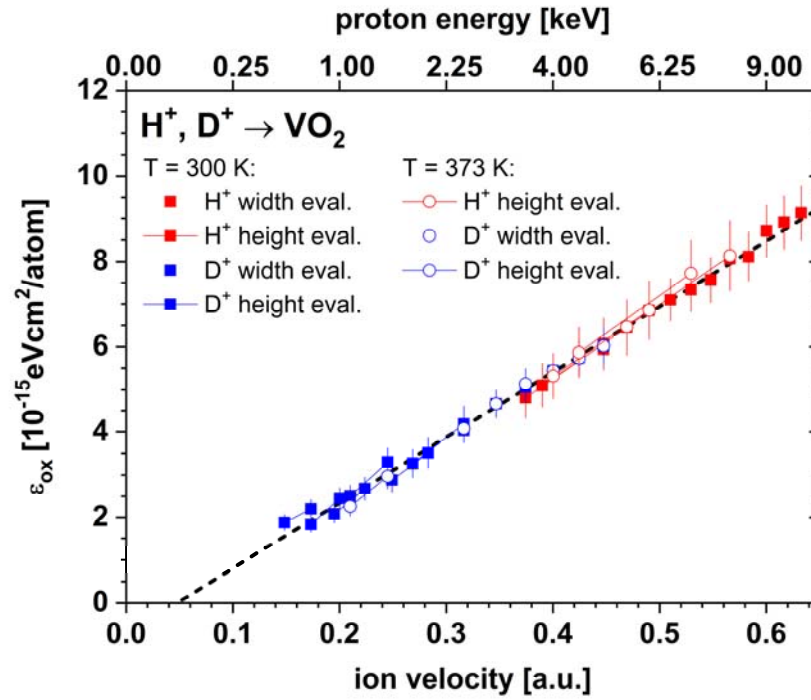
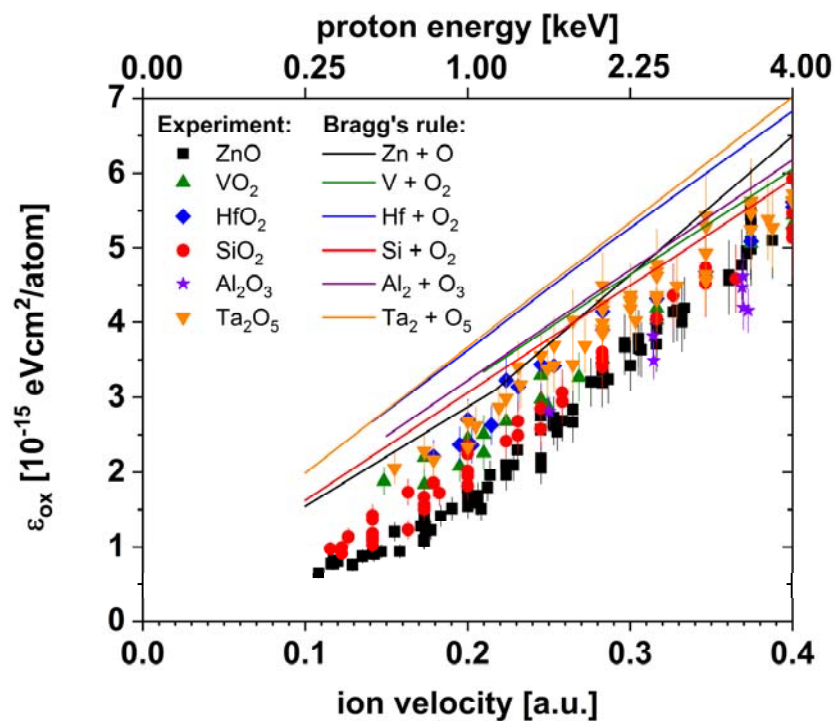


Fig. 1

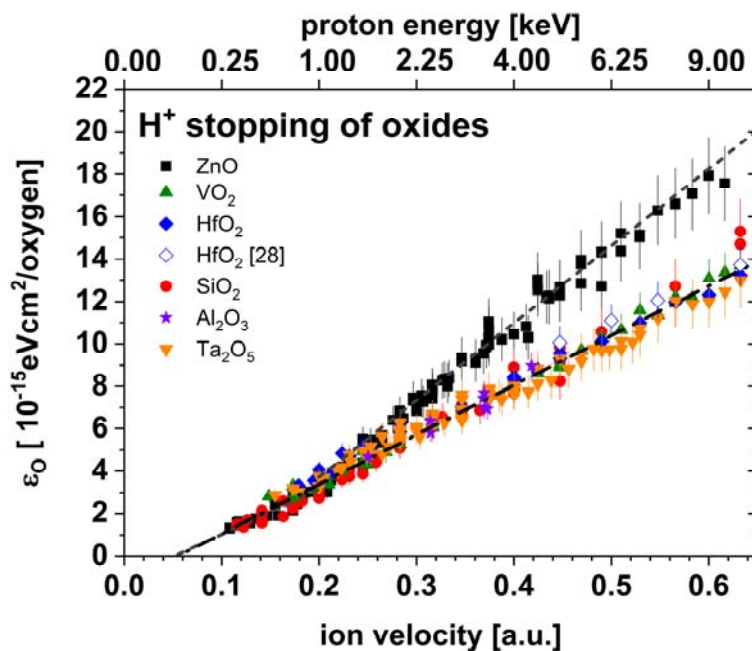
1



2

3

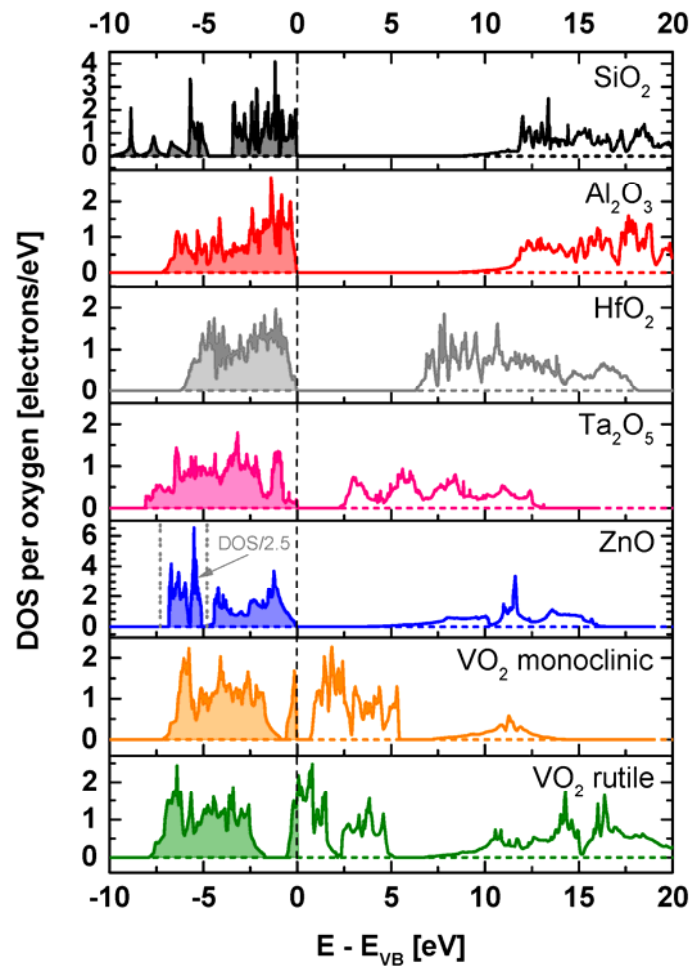
Fig. 2a



4

5

Fig. 2b



1  
2  
3

Fig. 3